BRAIN CONNECTIVITY
Volume 10, Number 1, 2020

DOI: 10.1089/brain.2019.0713

Human Brain Functional Network Organization Is Disrupted After Whole-Brain Radiation Therapy

Timothy J. Mitchell,[1,*] Benjamin A. Seitzman,[2,*] Nicholas Ballard,[1] Steven E. Petersen,[2–6] Joshua S. Shimony,[3] and Eric C. Leuthardt[4,5,7–10]

Abstract

Radiation therapy (RT) plays a vital role in the treatment of brain cancers, but it frequently results in cognitive decline in the patients who receive it. Because the underlying mechanisms for this decline remain poorly understood, the brain is typically treated as a single, uniform volume when evaluating the toxic effects of RT plans. This ignorance represents a significant deficit in the field of radiation oncology, as the technology exists to manipulate dose distributions to spare regions of the brain, but there exists no body of knowledge regarding what is critical to spare. This deficit exists due to the numerous confounding factors that are frequently associated with radiotherapy, including the tumors themselves, other treatments such as surgery and chemotherapy, and dose gradients across the brain. Here, we present a case in which a 57-year-old male patient received a uniform dose of radiation across the whole brain, did not receive concurrent chemotherapy, had minimal surgical intervention and a small tumor burden, and received resting-state functional magnetic resonance imaging (fMRI) scans both before and after RT. To our knowledge, this is the first study on the effects of whole-brain radiotherapy on functional network organization, and this patient's treatment regimen represents a rare and non-replicable opportunity to isolate the effects of radiation on functional connectivity. We observed substantial changes in the subject's behavior and functional network organization over a 12-month timeframe. Interestingly, the homogenous radiation dose to the brain had a heterogeneous effect on cortical networks, and the functional networks most affected correspond with observed cognitive behavioral deficits. This novel study suggests that the cognitive decline that occurs after whole-brain radiation therapy may be network specific and related to the disruption of large-scale distributed functional systems, and it indicates that fMRI is a promising avenue of study for optimizing cognitive outcomes after RT.

Keywords: cognition; cognitive dysfunction; executive function; functional magnetic resonance imaging; radiation dosage; radiotherapy

Introduction

Radiation therapy (RT) is frequently used in the treatment of both primary and metastatic brain cancer, with an estimated 200,000 patients per year in the United States receiving RT to the brain (Greene-Schloesser et al., 2013). Due to recent improvements in treatment techniques, these patients are surviving longer (Jensen et al., 2011), with ~100,000 of these patients surviving long enough to experience the deleterious effects of radiation to the brain (Greene-Schloesser et al., 2012). Approximately 50–90% of survivors experience some form of cognitive dysfunction after RT, and

Departments of [1]Radiation Oncology and [2]Neurology, Washington University in St. Louis–School of Medicine, St. Louis, Missouri.
[3]Mallinckrodt Institute of Radiology, Washington University in St. Louis–School of Medicine, St. Louis, Missouri.
[4]Department of Neuroscience, Washington University in St. Louis–School of Medicine, St. Louis, Missouri.
[5]Department of Biomedical Engineering, Washington University in St. Louis–School of Engineering and Applied Science, St. Louis, Missouri.
[6]Department of Psychological and Brain Sciences, Washington University in St. Louis, St. Louis, Missouri.
[7]Department of Mechanical Engineering and Materials Science, Washington University in St. Louis–School of Engineering and Applied Science, St. Louis, Missouri.
[8]Center for Innovation in Neuroscience and Technology and [9]Brain Laser Center, Washington University in St. Louis–School of Medicine, St. Louis, Missouri.
[10]Department of Neurological Surgery, Washington University in St. Louis–School of Medicine, St. Louis, Missouri.
*These authors contributed equally to this work.

the effects typically follow a biphasic process. First, patients experience a transient decline in memory beginning as early as 3 months after treatment. Second, patients experience a progressive, irreversible decline in cognitive ability from roughly a year onward (Makale et al., 2016). The mechanisms behind this cognitive decline are not fully understood, but they are likely multifaceted and synergistic. After radiation, changes have been observed in astrocytes, oligodendrocytes, mature neurons, neurogenesis, white matter, inflammation, and the vasculature (Greene-Schloesser et al., 2012). However, little is known about changes that occur at larger spatial scales, including the network level.

Functional magnetic resonance imaging (fMRI) measures the ratio of oxyhemoglobin to deoxyhemoglobin—the blood oxygen level-dependent (BOLD) signal—across the entire brain. Although its exact origins remain elusive, the BOLD signal has been shown to relate to bulk synaptic neural activity (Logothetis et al., 2001). In particular, resting-state (rs) fMRI measures spontaneous low-frequency (<0.1 Hz) oscillations in the BOLD signal that are present in the absence of any directed task or sensory input. These oscillations exhibit synchrony within widely distributed regions of the brain that are known as functional networks. Functional networks map onto distinct anatomical and functional systems of the brain, including sensory systems (e.g., motor, visual) and more recently observed higher-level cognitive systems (Biswal et al., 1995; Fox et al., 2005; Power et al., 2011; Seeley et al., 2007). Moreover, functional networks have been shown to be related to cognition (Sheffield et al., 2017) and altered in disorders such as depression (Sheline et al., 2009), autism (Anderson et al., 2011), stroke (Siegel et al., 2016), schizophrenia (Sheffield et al., 2015), and neurodegenerative diseases (Seeley et al., 2009).

This article details changes in functional network organization found in a patient who received whole-brain radiation therapy (WBRT), in which the entire brain receives a uniform dose of radiation. WBRT has been associated with larger cognitive dysfunction than focal radiotherapy treatments in the brain, beginning in as little as 3 months (Brown et al., 2016). We collected rs-fMRI data from the patient 3 weeks before RT and 9 months post-RT onset in addition to standard clinical measures of cognitive function. Uniquely, this patient did not receive chemotherapy at the time of WBRT, which removes a common confounding variable for relating changes in functional network organization due to radiotherapy with cognitive decline. In addition, the patient was imaged both before and after WBRT, meaning that changes in functional network organization can be studied by using a within-subject control in addition to comparison against a population of healthy controls. Further, because the patient received WBRT rather than focal irradiation, each distributed functional network was irradiated to the same dose level of 37.5 Gy. Finally, no new lesions were found at the time the second set of fMRI data was collected, so any changes due to tumor progression should be minimal. This case presents a unique opportunity to investigate the effects of a uniform dose of radiation on individual functional networks and how those effects correlate with changes in behavior.

Patient History

The patient presented as a 57-year-old right-handed male with memory problems developing over the previous 4 weeks as well as right-sided numbness in his leg and mild incoordination of his right hand. He described the memory problems as a processing issue in which, for example, he would attempt to make a cup of coffee, but would be unable to remember the necessary sequence to do so, and would ultimately move on without having completed the task. The patient had previously been in good health. Subsequent computed tomography (CT) and MR scanning revealed a deep left frontal lobe enhancing mass involving the dorsomedial anterior thalamus with extensive surrounding T2-weighted FLuid Attenuated Inversion Recovery (T2/FLAIR) hyperintensity (Fig. 1). A 3-mm left cerebellar lesion was also noted. A biopsy confirmed metastatic adenocarcinoma, but positron emission tomography and CT workup were unable to identify a primary malignancy in the chest, abdomen, or pelvis.

Before an MRI-guided laser ablation procedure to treat the left frontal lesion, the patient underwent neurocognitive testing with a Montreal Cognitive Assessment (MOCA) exam (Table 1). Two weeks later, the patient began a course of WBRT. The treatment utilized 6 MV photons to a total dose of 37.5 Gy

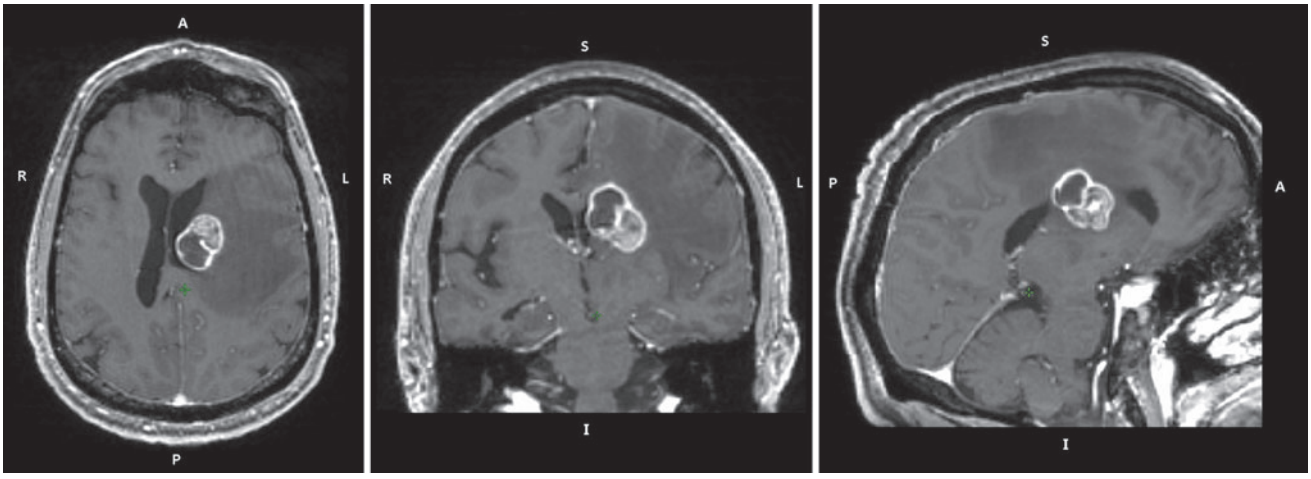

FIG. 1. Pre-treatment patient anatomy. A T1-weighted anatomical image obtained 19 days before RT onset is displayed. A large (2.9 × 2.3 × 2.9 cm) tumor is present in the deep left frontal lobe, as well as significant edema in the left hemisphere. RT, radiation therapy.

Table 1. Montreal Cognitive Assessment Results

	3 Weeks before WBRT onset	*11.5 Months after WBRT onset*
Executive function/ visuoconstructional skills	5	3
Naming	3	2
Attention/calculations	5	1
Language	1	2
Abstraction	2	2
Memory	1	0
Orientation	5	3
Total	22	13

The results of the Montreal Cognitive Assessment, a standard clinical assessment of cognitive function, are displayed both before WBRT and after WBRT. The patient experienced substantial cognitive decline over the course of 11.5 months after radiation therapy onset.

WBRT, whole-brain radiotherapy.

(35.5–40.5 Gy range) delivered in 15 fractions of 2.5 Gy per fraction. The treatment was completed in a total of 21 days.

An MRI taken 2.5 months after the start of RT noted only post-treatment changes to the left frontal lesion. The left cerebellar lesion was no longer well visualized, and this would remain the case throughout the course of treatment. An MRI acquired 5.5 months post-RT noted a new lateral rim of contrast enhancement surrounding the laser ablation cavity, and a thickening of this enhancement found on MRI 8 months post-RT indicated recurrence. A second laser ablation was performed nearly 9 months post-RT, and the second fMRI dataset was acquired the next day. After all functional imaging was acquired, the patient received four cycles of Carbo/Alimta. A second MOCA exam was administered 11.5 months after the start of radiotherapy (Table 1). No primary disease site was identified. See Figure 2 for the full timeline of treatment and data acquisition.

Methods

Patient dataset

Dataset characteristics. The Washington University Internal Review Board approved the study. Eyes-open rs-fMRI data were collected from the patient (M, right handed, 57 years old) 3 weeks before and 9 months after the onset of RT (time points 1 and 2, respectively).

Data acquisition. A Siemens MAGNETOM Tim TRIO 3.0T MRI scanner and a 12-channel Head Matrix Coil were used to obtain T1-weighted (magnetization-prepared rapid gradient-echo [MP-RAGE], 1.9 s TR, 2.53 ms TE, $1\times1\times1$ mm voxels) and BOLD contrast-sensitive (gradient echo planar imaging [EPI], 2.2 s TR, 27 ms TE, $4\times4\times4$ mm voxels) images at each time point. Because there were multiple such scanners available at the time of scanning, it is not known whether the scans for time point 1 and time point 2 were acquired on the same scanner. However, acquisition parameters were identical, and recent work by Ciric and colleagues (2017) demonstrated that most artifacts in resting-state data, particularly those related to head motion, are ameliorated by the processing pipeline described in the Preprocessing and Correlation Matrix section. The amount of BOLD data acquired per run was 160 frames (5.87 min). Three runs were acquired at time point 1, and two runs were acquired at time point 2. Thus, 17.6 min of data were acquired at time point 1 and 11.7 min of data were acquired at time point 2. The patient was instructed to fixate on a black crosshair presented at the center of a white background.

Preprocessing and correlation matrix. The data from each time point were processed separately. Except where explicitly stated, all preprocessing steps were performed by using the 4dfp software package developed at Washington University in St. Louis (https://4dfp.readthedocs.io/en/latest/). For each time point, the first 12 frames (30 sec) of each run were discarded to account for magnetization equilibrium and an auditory evoked response at the start of the EPI sequence (Laumann et al., 2015). Slice timing correction was applied first. Then, all functional data were aligned to the first frame of the first run by using rigid body transforms. The aligned data were normalized such that the whole-brain mode intensity value was 1000 (Miezin et al., 2000). Next, the data were resampled (3 cubic mm voxels), motion corrected, and registered to the T1-weighted image from time point 2 (the T1-weighted image from time point 1 caused several registration errors due to edema; see Fig. 1). Finally, the patient's data were aligned to the Talairach atlas (Ojemann et al., 1997) by using affine transforms for an aberrant functional connectivity (AFC) analysis against a set of controls (described in the Aberrant Functional Connectivity

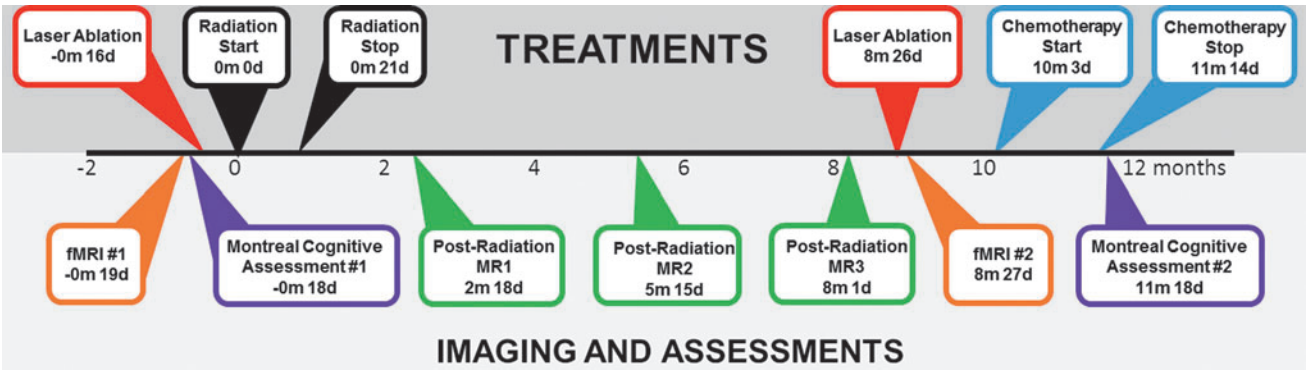

FIG. 2. Timeline of treatment, imaging, and cognitive assessments. The time of each MRI, treatment, and cognitive assessment is shown relative to RT onset (±months and days). MRI, magnetic resonance imaging.

Analysis section). Resampling, motion correction, and registration were performed by using a one-step operation (Smith et al., 2004).

Additional preprocessing of the functional data was applied to remove artifacts that are particularly problematic for resting-state BOLD (Ciric et al., 2017; Power et al., 2014). Frame-wise displacement (FD) was calculated as in Power and colleagues (2012), but first the six head motion parameters that compose FD were lowpass filtered (0.1 Hz) to account for respiration artifacts (Fair et al., 2020; Siegel et al., 2017). Frames with ''filtered'' FD greater than 0.1 mm were censored, as were all uncensored segments with fewer than five contiguous frames. A total of 225 (8.25 min) and 211 (7.74 min) frames were retained at time points 1 and 2, respectively. Least-squares spectral estimation was implemented to interpolate over all censored frames (Hocke and Kämpfer, 2009; Power et al., 2014).

Next, the data were bandpass filtered from 0.009 to 0.08 Hz. Finally, a matrix of nuisance regressors was constructed to include the whole-brain mean (global) signal, white matter and ventricular cerebrospinal fluid signals, the temporal derivatives of each of these signals, and an additional 24 movement regressors derived by expansion (Friston et al., 1996; Satterthwaite et al., 2012; Yan et al., 2013). FreeSurfer 6.0 automatic segmentation was applied to the T1-weighted image from time point 2 to create a patient-specific mask of the gray matter, white matter, and ventricles for the regressors (Fischl et al., 2002). Finally, the data were smoothed by using a Gaussian smoothing kernel with a full width at half maximum of 6 mm (sigma = 2.55).

At the end of all preprocessing, each censored/interpolated frame was removed from the time series for all further analyses. The time series from each run (within a time point) were concatenated. Then, the mean BOLD signal from each of 300 regions of interest (ROIs) (Seitzman et al., 2020) was extracted. These ROIs are specifically designed for functional network analysis with whole-brain coverage, with each of the 300 ROIs being assigned to one of the functional networks listed in Figure 3E. The Pearson product-moment correlation was computed between each possible pair of these 300 time series to generate a 300×300 correlation matrix that can be seen in Figure 3A. This process was repeated for time point 2, which is shown in Figure 3B. Thus, two 300×300 correlation matrices were created. The matrices were sorted by functional networks defined *a priori* (Seitzman et al., 2020). Finally, we computed the difference between these two matrices (time point 1 − time point 2) for Figure 3C and F, as well as the absolute difference between the two matrices.

Healthy controls datasets

Two sets of healthy controls were used in this article—the WashU 120 and the Midnight Scan Club (MSC). The WashU 120 contains a large number of subjects, which is useful for an AFC analysis (described in the Aberrant Functional Connectivity Analysis section), whereas the MSC contains a small number of highly sampled individuals, which is useful for addressing the effects of sampling error (described in the Creation of a Null Model section).

Dataset characteristics. The WashU 120 dataset of healthy control subjects has been previously described (Power et al., 2011). Eyes-open rs-fMRI data were acquired from healthy, right-handed, native English speaking, young adults ($N = 120$, 60 F, age range 18–32, mean age 24.7 years old). Subjects were recruited from the Washington University community and included in the study only if they had no current or previous history of neurologic or psychiatric diagnosis as well as no head injuries resulting in a loss of consciousness for more than 5 min. Informed consent was obtained from all participants, and the Washington University Internal Review Board approved the study.

The MSC dataset of healthy control subjects has also been previously described (Gordon et al., 2017). Eyes-open rs-fMRI data were acquired from healthy, right-handed, native English speaking, young adults ($N = 10$, 5 F, age range 24–34, mean age 29.1 years old).

Data acquisition. A Siemens MAGNETOM Tim TRIO 3.0T MRI scanner and a 12-channel Head Matrix Coil were used to obtain T1-weighted (MP-RAGE, 2.4 s TR, $1 \times 1 \times 1$ mm voxels) and BOLD contrast-sensitive (gradient echo EPI, 2.5 s TR, $4 \times 4 \times 4$ mm voxels) images from each subject. The mean amount of BOLD data acquired per subject from the WashU 120 was 14 min (336 frames, range = 184–729 frames). For each MSC subject, a single 30-min BOLD run was acquired on 10 separate days (for a total of 5 h of data per subject). Subjects were instructed to fixate on a black crosshair presented at the center of a white background. See Power and colleagues (2011) and Gordon and colleagues (2017) for full acquisition details.

Preprocessing and correlation matrix. All preprocessing was identical to the processing described in the Preprocessing and Correlation Matrix section, except that FD was calculated as in Power and colleagues (2012). Thus, frames with ''unfiltered'' FD greater than 0.2 mm were censored (mean ± std frames retained = 279 ± 107). Time series were extracted from each of the ROIs mentioned earlier (the 300 from Seitzman et al., 2020) for each run (and for each subject). For the WashU 120, a 300×300 correlation matrix was created for each subject ($N = 120$) in the same manner as described earlier (the Preprocessing and Correlation Matrix section). For Figure 3D, a group-average was created after applying the Fisher Z-Transform to each individual matrix (to create a normal distribution of values), averaging all matrices, and, finally, applying the inverse Fisher Z-Transform.

FIG. 3. Substantial changes in functional network organization after whole-brain radiation therapy. Correlation matrices represent the patient's functional network organization pre-WBRT **(A)** and 8 months post-WBRT **(B)**. Functional networks are color-coded as displayed on the brain shown in **(E)**. The difference matrix was calculated as pre-WBRT minus post-WBRT, and a conservative null model was used to eliminate the effects of sampling variability. The bottom triangle of the matrix **(C)** shows correlation differences that survived the null model. The blue (pre<post) and yellow (pre>post) blocks in the upper triangle of the matrix in **(C)** represent mean network-wise (block-level) changes. The within-network changes from **(C)** are plotted on the brain in **(F)**. For reference, the health adult group average from the Midnight Scan Club is shown in **(D)**.

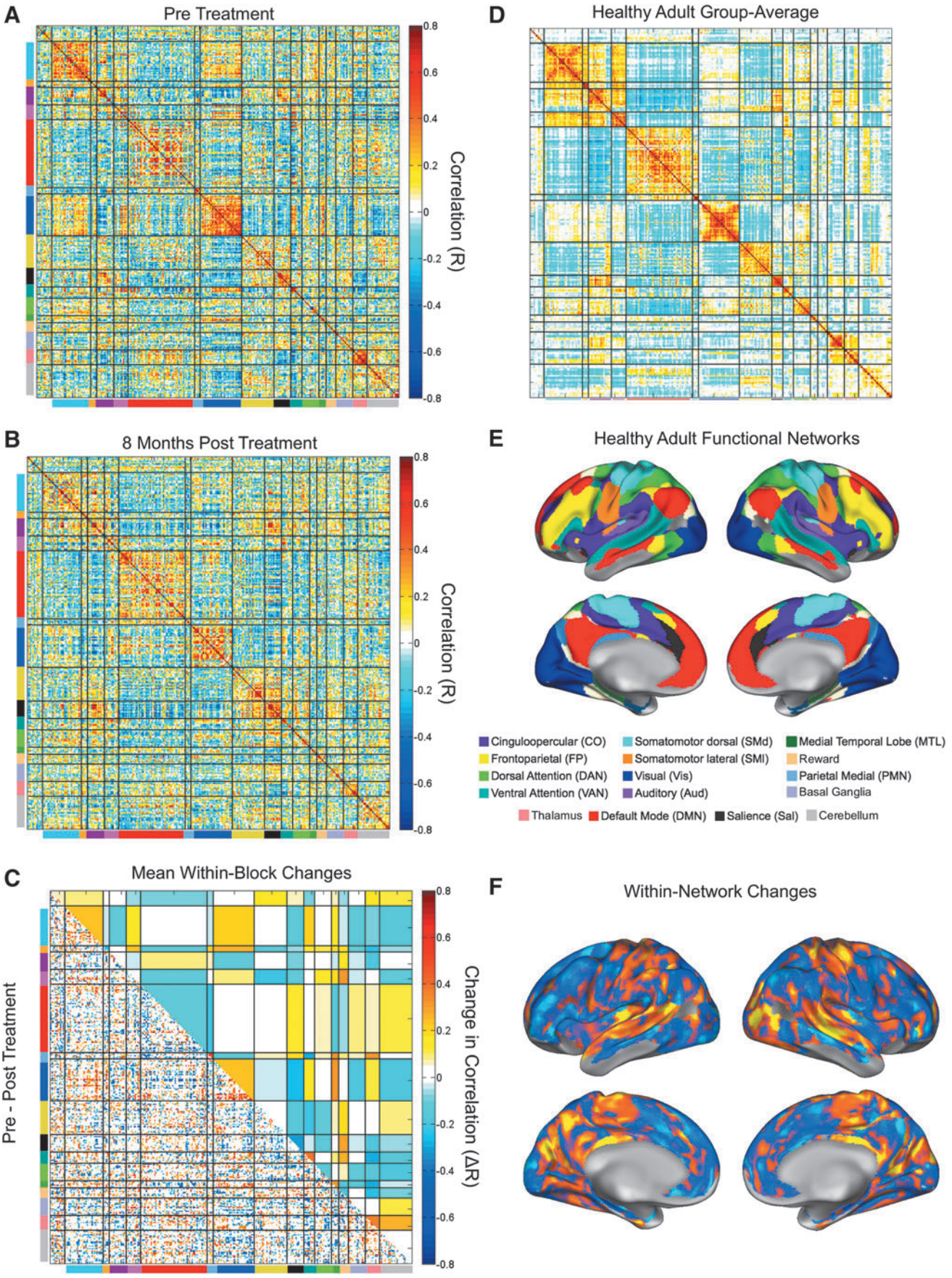
A
Pre Treatment
0.8
0.6
0.4
0.2
0
-0.2
-0.4
-0.6
-0.8
Correlation (R)
B
8 Months Post Treatment
0.8
0.6
0.4
0.2
0
-0.2
-0.4
-0.6
-0.8
Correlation (R)
C
Mean Within-Block Changes
Pre - Post Treatment
0.8
0.6
0.4
0.2
0
-0.2
-0.4
-0.6
-0.8
Change in Correlation (ΔR)
D
Healthy Adult Group-Average
E
Healthy Adult Functional Networks
Cinguloopercular (CO)
Somatomotor dorsal (SMd)
Medial Temporal Lobe (MTL)
Frontoparietal (FP)
Somatomotor lateral (SMl)
Reward
Dorsal Attention (DAN)
Visual (Vis)
Parietal Medial (PMN)
Ventral Attention (VAN)
Auditory (Aud)
Basal Ganglia
Thalamus
Default Mode (DMN)
Salience (Sal)
Cerebellum
F
Within-Network Changes

Creation of a null model

Since the patient had a small amount of data relative to the amount required for reliable individual-specific functional network analyses (Gordon et al., 2017; Laumann et al., 2015), a null model was generated to account for sampling error. The publicly available MSC (Gordon et al., 2017) dataset was used to do so.

Within each subject, a randomly chosen 8-min segment of good (uncensored) BOLD data was sampled from two randomly chosen runs. The segments were chosen to be 8 min long because that is the approximate amount of good (uncensored) BOLD data retained from the patient's data at each time point. Then, two correlation matrices were created (one per 8-min segment) as described in the Preprocessing and Correlation Matrix section, and the difference between the two matrices was computed. This process was repeated (for each MSC subject) 1000 times. Thus, a null distribution was created, reflecting expected within-subject correlation differences attributable to sampling error (i.e., creating matrices with only 8-min of good BOLD data) and day-to-day variation (all MSC runs were collected at midnight, so there are minimal circadian effects). The distribution of sampling-error differences in correlation ranged from −0.25 to +0.25 (Supplementary Fig. S1). To be conservative, all entries within this range in the patient's difference matrix (time point 1 − time point 2) were set to 0.

AFC analysis

To test for further effects of WBRT on functional networks, the approach developed by Siegel and colleagues (2014) to compare functional connectivity from a single patient with a distribution of healthy controls (the so-called AFC) was also implemented. Briefly, for each ROI, a seedmap was created (the correlation between the ROI timeseries and all other ROI timeseries) for each healthy control subject, yielding a distribution of seedmaps for each ROI across healthy control subjects. This process was repeated for each ROI for the patient, and the patient's individual seedmaps were then compared with the distribution of healthy control seedmaps to acquire a metric of aberrancy known as the sensitivity metric (Swets et al., 1961). Moreover, this analysis was adapted to be able to do network-specific comparisons. Thus, all seedmaps within a functional network were averaged together for each subject (e.g., all seedmaps within the visual network were averaged together within a subject). Thus, the control–control and patient–control distributions represent functional network differences rather than ROI differences.

Unaffected hemisphere only

All of the aforementioned analyses were repeated while excluding the left hemisphere (which contained the large tumor and edema). The single hemisphere analysis results can be found in Supplementary Figures S2 and S3 for reference and are similar to the whole-brain analysis results presented here.

Results

The patient experienced significant cognitive decline

The patient initially presented with memory impairment, and this was confirmed on the initial MOCA assessment with a memory score of 1/5. Using a cutoff of 26 on the total MOCA score to define cognitive impairment (Nasreddine et al., 2005), the patient exhibited cognitive impairment both 3 weeks before WBRT and 11 months after WBRT onset (Table 1). After WBRT, the patient demonstrated additional cognitive decline, with the total MOCA score falling from 22 to 13. The declines occurred in multiple cognitive domains, including executive function/visuo-constructional skills (5–3), naming (3–2), attention/calculations (5–1), memory (1–0), and orientation (5–3). The language domain showed a mild improvement (1–2), and abstraction was unchanged (2).

WBRT caused substantial changes in functional network organization

Functional networks, which consist of widely distributed regions of the brain that exhibit a high degree of synchrony in BOLD signal, can be mapped onto distinct anatomical areas of the brain (Fig. 3E). In healthy controls, this strong within-network BOLD signal synchrony can be observed as on-diagonal blocks of large, positive correlations, as seen in the correlation matrix in Figure 3D. The patient under study here demonstrated such organization pre-WBRT (Fig. 3A), but this organization was disrupted significantly post-WBRT (Fig. 3B). To quantify these effects, we computed a difference matrix and applied a conservative null model to determine significant changes (see the Creation of a Null Model section and Supplementary Fig. S1). The seed regions (Fig. 3C, bottom-left triangle) and networks (Fig. 3C, top-right triangle) that changed significantly are plotted, whereas those that failed to meet significance are blank. For spatial reference, the within-network changes are plotted on the brain in Figure 3F.

The AFC analysis was performed on the pre- and post-radiation data to determine how the patient's functional connectivity changed relative to controls. The visual network is displayed as an exemplar in Figure 4A. Correlation values closer to one indicate that the patient's visual network was more similar to the visual network of controls, whereas values closer to zero indicate minimal relationship with controls. It is evident from the low patient-to-control correlations in both distributions that the visual network in the patient was aberrant both pre- and post-radiation, but the post-radiation distribution became more aberrant relative to controls. We measured the difference between the pre- and post-radiation distributions using a d' (i.e., sensitivity) metric, where a larger d' value reflects a larger separation between the two distributions. We observed that most networks became more aberrant after radiotherapy, but that specific functional networks were more sensitive to radiation changes in the context of this patient-to-control comparison (Fig. 4B). Specifically, we discovered that the medial temporal lobe (MTL) network (composed of the anterior portion of the hippocampus and entorhinal cortex) and the frontoparietal (FP) network (yellow network in Fig. 3E) were most sensitive to these changes.

Discussion

Though this is a single case study, this work highlights a fundamental and important phenomenon associated with WBRT: WBRT delivers a homogeneous dose of radiation to the brain, but the impact on the brain's cortical networks is heterogeneous. In particular, relative to other networks, both the MTL and FP control networks appear to be more altered

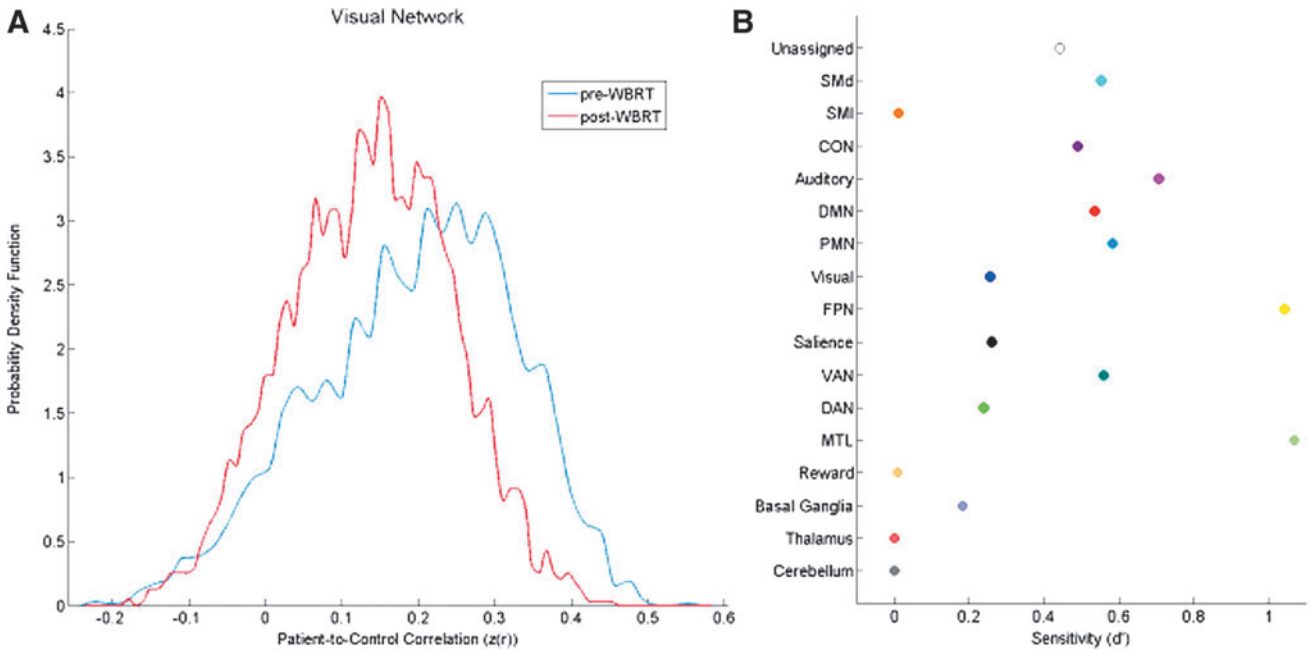

FIG. 4. z-Scored correlation coefficient distribution across ROIs (left) and network sensitivity to radiation (right). The Aberrant Functional Connectivity Analysis presented here follows the approach developed by Siegel and colleagues (2014) to compare functional connectivity from a single patient with a population of healthy controls. The distribution of the patient's z-scored correlation coefficients for all ROIs in the visual network is shown in **(A)** for both the pre- (blue) and post-radiation (red) scans. The change in the patient's functional connectivity from pre- to post-radiation relative to controls is represented by the sensitivity metric d' for each network in **(B)** (Swets et al., 1961). The frontoparietal network (yellow) and medial temporal lobe network (light green) were the most sensitive ($d' > 1$). ROI, region of interest.

from exposure to the same dose of radiation. The existence of network-level variability in response to radiotherapy may prove to be an important consideration in the formulation of radiotherapy plans that optimize patient outcomes.

RT plans an important role in the management of both primary and metastatic brain tumors. The goal of any RT treatment is to optimize the therapeutic ratio, which is the balance between the probability of tumor control and the risk of damage to normal tissue. Achieving this goal can be difficult in RT because the doses required to treat the tumor at the therapeutic level often require normal tissue to receive levels of dose that can cause complications. Presently, an estimated 50–90% of patients receiving RT to the brain will experience some form of cognitive dysfunction, the most common complication of RT to the brain (Makale et al., 2016). Although this unwanted dose to normal tissue is inevitable, modern radiotherapy techniques allow for the delivery of radiation dose distributions that are highly conformal to the tumor while sparing nearby critical structures. Despite this ability to ''dose paint,'' the brain is largely still treated as a single, uniform volume, with toxicity metrics focused on dose–volume effects rather than the physical location of the dose (Lawrence et al., 2010). The reason behind this simplistic model of the brain is that the underlying mechanisms behind the cognitive dysfunction post-RT are poorly understood. Beyond critical structures such as those necessary for vision and the brainstem, there is little evidence to suggest that particular regions of the brain are more sensitive to radiation than others. Recently, some structural partitioning of the brain has taken place, with studies investigating the effects of hippocampal sparing on memory (Gondi et al., 2014). However, many functions, including higher-level cognitive functions, are widely distributed and require a network-level perspective.

Case summary: broad cognitive decline and functional connectivity changes

The patient experienced a sharp decline in cognitive function in the year after WBRT, with his MOCA score declining from 22 to 13. The cognitive decline observed here is complicated by the patient receiving chemotherapy over 41 days, starting 45 days before collection of the second MOCA, because chemotherapy is known to affect cognitive functions (Tannock et al., 2004). Though chemotherapy may play an additional role in the patient's functional status at the time of the administration of the second MOCA, the observed cognitive decline is consistent with known effects of radiation to the brain. Douw and colleagues (2009) found that patients who were treated using RT for low-grade glioma performed worse in measures of attentional functioning, executive functioning, and information processing speed than patients who did not receive RT in their course of treatment. This finding agrees with the patient's most drastic change occurring in the Attentions/Calculations portion of the exam, as the patient's score decreased from 5 to 1 in this domain. Likewise, Gregor and colleagues (1996) found that patients treated with WBRT scored lower on visuospatial organization, visual memory, and complex information processing than patients treated with focal irradiation. For a review of the cognitive domains most affected by RT, as well as the tests used to assess cognitive function, see work by McDuff and colleagues (2013).

The patient's cognitive decline after RT was accompanied by a corresponding disruption in functional network organization. It should be noted that although chemotherapy may have affected the patient's cognitive testing, it was not a factor in the observed functional network changes, as the chemotherapy treatment did not begin until after the date of the second fMRI acquisition. In the limited number of studies to explore functional connectivity in RT patients, others have found evidence of functional connectivity changes post-RT. In patients treated with RT for glioblastoma, changes in task-based connectivity within the motor and auditory areas were shown to correlate with high-dose regions (Kovács et al., 2015). In addition, Ma and colleagues (2016) were able to successfully distinguish between nasopharyngeal carcinoma patients treated with or without RT based on changes in fMRI correlations. However, both these studies focused on specific networks or individual seed regions due to the focal nature of the radiation delivered. In contrast, this study focused on a patient receiving a uniform dose of radiation throughout the entire brain, allowing for the investigation into global effects, as well as individual networks' susceptibility to changes post-RT. Indeed, all networks contained seed regions that showed changes larger than would be expected from sampling variability (Fig. 3C). Interestingly, specific networks, particularly the MTL network and the FP control network, were affected more than other networks by WBRT.

MTL network

The hippocampus, which along with the entorhinal cortex comprises the MTL network, is critical for formation of episodic memories, trace conditioning, declarative memory, and spatial navigation (Fortin et al., 2002; Henke et al., 1999). There is increasing evidence that the hippocampus and surrounding cortex play an important role in the cognitive decline of patients receiving intracranial RT. After RT, patients frequently exhibit memory impairment (Gregor et al., 1996; Laukkanen et al., 1988; Welzel et al., 2008), and studies have demonstrated that hippocampal dosimetry correlates with changes in neurocognitive function (Gondi et al., 2013; Tsai et al., 2015). In addition, recent studies that explicitly spare the hippocampus during whole-brain radiotherapy have demonstrated a reduced decline on the Hopkins Verbal Learning Test-Revised when compared with WBRT without hippocampal sparing (Gondi et al., 2014). The results of this study offer additional evidence for the importance of the hippocampus in radiation-induced cognitive decline, as the MTL network showed the largest change from pre- to post-RT out of all networks studied (Fig. 4). The prevailing theory behind hippocampal impairment post-RT is a reduction in hippocampal neurogenesis (Makale et al., 2016). However, the results shown here indicate that there may be a large-scale, network-level component in addition to the observed cellular changes in the hippocampus.

FP control network

The FP network, which consists of dorsolateral and dorsomedial prefrontal cortex, part of the inferior parietal lobule and intraparietal sulcus, and the posterior portion of the middle temporal gyrus, is the second network to show large changes after RT. For a comprehensive review of the FP network, see Marek and Dosenbach (2019). In short, it is a widely distributed functional network that is believed to exert top–down control over and coordination of multiple functional networks to both initiate and adapt goal-directed task performance (Cole et al., 2013; Dosenbach et al., 2006, 2007). It is an important component of the so-called cortico-thalamic-cerebellar-cortico loop, which is believed to be integral for task control (Ide and Li, 2011). The strength of the within-FP correlations has been shown to relate to performance on cognitive tasks (Rypma et al., 2006; Song et al., 2008), and it is believed to play a critical role in mental health, with changes in the FP network having been observed in diseases such as schizophrenia and psychotic bipolar disorder (Sheffield et al., 2015).

The patient's within-FP correlations were already disrupted before WBRT relative to a distribution of healthy controls, which is consistent with the initial presentation of cognitive impairment. One explanation that we did not observe further within FP disruption after WBRT is the floor effect (the network may have already been maximally affected). Regardless, correlations between the FP and other networks changed significantly as a result of WBRT, especially between the FP and the cerebellum, the dorsal attention network, and the ventral attention network. If the FP plays a role in controlling and coordinating the functions of other networks, then loss of correlations between the FP and the attention systems of the brain could explain the substantial decline observed in the attention/calculations domain. Likewise, disruption of the relationship between the FP and cerebellum may explain the observed cognitive decline. Conversely, the changes in executive function observed in both this patient and other studies may, in fact, be a secondary effect of the more frequently observed memory impairment after brain radiotherapy. Though this study indicates that the FP network is affected by WBRT, its precise role in the cognitive changes post-WBRT remains to be elucidated. Further understanding of the role of the FP network in WBRT is crucial, as FP sparing may provide an opportunity to improve cognition after radiotherapy.

Limitations and conclusions

This article investigates changes in resting-state functional network organization in a single patient. Though reliable network identification is possible in individual subjects (Hacker et al., 2013), individual variability in cognitive architecture presents a challenge. By using the subject as his own control, we minimized this potential issue. Converging evidence from additional studies would provide important arbitration over the presented conclusions.

There are several confounds that make isolating the specific effects of radiation on cognitive function difficult. First, the tumors themselves can affect functional network organization (Harris et al., 2014). In this particular case, the patient's functional connectivity was abnormal before receiving radiotherapy (Fig. 4A). Second, radiation is rarely the only treatment method employed for cranial lesions. In this study, the patient had two focal laser ablations to treat the thalamic tumor, which involves placing a wide needle into the brain to provide direct access to the tumor. Uniquely, this patient did not receive chemotherapy as part of his course of treatment during the period between his two rs-fMRI dates. Thus, over the course of the 9.5 months between rs-fMRI scans, one would expect the patient's functional connectivity to be altered by the two laser ablations, the tumor recurrence, and the radiation. To isolate the effects of the radiation, we performed the analysis on the right hemisphere only,

which did not have a tumor and was not touched during the focal laser ablation on the left. We found similar results to all analyses performed on the whole brain, which suggests that the observed changes resulted from radiation. Finally, for the patient-control AFC analysis, we used healthy controls that were younger than the patient and were 50% female. However, we chose this dataset because their acquisition parameters, scanner type, and study location were nearly identical to the patient's.

Despite these limitations, this article offers evidence in favor of the utility of rs-fMRI in understanding the effects of radiation on functional network organization. Our results suggest that the cognitive decline that occurs after WBRT may be related to disruption of the brain's large-scale, distributed functional systems. Additional studies are needed to understand these disruptions in full, and they may provide insight into how to optimize the clinical efficacy of RT while minimizing cognitive decline.

Author Disclosure Statement

E.C.L. declares the following conflicts: Neurolutions and Inner Cosmos. All other authors declare no conflicts of interest.

Funding Information

This work was supported by National Institutes of Health grants T32 NS073547 (BAS), R01 NS32979 (SEP), R01 NS06424 (SEP), R01 CA203861 (ECL), and R44 GM125438 (ECL); the Hope Center for Neurological Disorders (SEP); the James S. McDonnell Foundation Grant 220020534 (SEP) and Collaborative Activity Award (SEP); JSS was supported by the Eunice Kennedy Shriver National Institute Of Child Health & Human Development of the National Institutes of Health under Award Number U54 HD087011 to the Intellectual and Developmental Disabilities Research Center at Washington University. TJM and NB received no funding.

Supplementary Material

Supplementary Figure S1
Supplementary Figure S2
Supplementary Figure S3

References

Anderson JS, Druzgal TJ, Froehlich A, Dubray MB, Lange N, Alexander AL, et al. 2011. Decreased interhemispheric functional connectivity in autism. Cereb Cortex 21:1134–1146.

Biswal B, Yetkin FZ, Haughton VM, Hyde JS. 1995. Functional connectivity in the motor cortex of resting human brain using echo-planar MRI. Magn Reson Med 34:537–541.

Brown PD, Jaeckle K, Ballman KV, Farace E, Cerhan JH, Anderson SK, et al. 2016. Effect of radiosurgery alone vs radiosurgery with whole brain radiation therapy on cognitive function in patients with 1 to 3 brain metastases: a randomized clinical trial. JAMA 316:401–409.

Ciric R, Wolf DH, Power JD, Roalf DR, Baum GL, Ruparel K, et al. 2017. Benchmarking of participant-level confound regression strategies for the control of motion artifact in studies of functional connectivity. Neuroimage 154:174–187.

Cole MW, Reynolds JR, Power JD, Repovs G, Anticevic A, Braver TS. 2013. Multi-task connectivity reveals flexible hubs for adaptive task control. Nat Neurosci 16:1348–1355.

Dosenbach NUF, Fair DA, Miezin FM, Cohen AL, Wenger KK, Dosenbach RAT, et al. 2007. Distinct brain networks for adaptive and stable task control in humans. Proc Natl Acad Sci U S A 104:11073–11078.

Dosenbach NUF, Visscher KM, Palmer ED, Miezin FM, Wenger KK, et al. 2006. A core system for the implementation of task sets. Neuron 50:799–812.

Douw L, Klein M, Fagel SSAA, van den Heuvel J, Taphoorn MJB, Aaronson NK, et al. 2009. Cognitive and radiological effects of radiotherapy in patients with low-grade glioma: long-term follow-up. Lancet Neurol 8:810–818.

Fair DA, Miranda-Dominguez O, Snyder AZ, Perrone AA, Earl EA, Van AN, et al. 2020. Correction of respiratory artifacts in MRI head motion estimates. Neuroimage 208:116400. DOI: 10.1016/j.neuroimage.2019.116400.

Fischl B, Salat DH, Busa E, Albert M, Dieterich M, Haselgrove C, et al. 2002. Whole brain segmentation: automated labeling of neuroanatomical structures in the human brain. Neuron 33:341–355.

Fortin NJ, Agster KL, Eichenbaum HB. 2002. Critical role of the hippocampus in memory for sequences of events. Nat Neurosci 5:458–462.

Fox MD, Snyder AZ, Vincent JL, Corbetta M, Van Essen DC, Raichle ME. 2005. The human brain is intrinsically organized into dynamic, anticorrelated functional networks. Proc Natl Acad Sci U S A 102:9673–9678.

Friston KJ, Williams S, Howard R, Frackowiak RS, Turner R. 1996. Movement-related effects in fMRI time-series. Magn Reson Med 35:346–355.

Gondi V, Hermann BP, Mehta MP, Tomé WA. 2013. Hippocampal dosimetry predicts neurocognitive function impairment after fractionated stereotactic radiotherapy for benign or low-grade adult brain tumors. Int J Radiat Oncol Biol Phys 85:348–354.

Gondi V, Pugh SL, Tome WA, Caine C, Corn B, Kanner A. 2014. Preservation of memory with conformal avoidance of the hippocampal neural stem-cell compartment during whole-brain radiotherapy for brain metastases (RTOG 0933): a phase II multi-institutional trial. J Clin Oncol 32:3810–3816.

Gordon EM, Laumann TO, Gilmore AW, Newbold DJ, Greene DJ, Berg JJ, et al. 2017. Precision functional mapping of individual human brains. Neuron 95:791–807.e797.

Greene-Schloesser D, Moore E, Robbins ME. 2013. Molecular pathways: radiation-induced cognitive impairment. Clin Cancer Res 19:2294–2300.

Greene-Schloesser D, Robbins ME, Peiffer AM, Shaw EG, Wheeler KT, Chan MD. 2012. Radiation-induced brain injury: a review. Front Oncol 2:73.

Gregor A, Cull A, Traynor E, Stewart M, Lander F, Love S. 1996. Neuropsychometric evaluation of long-term survivors of adult brain tumours: relationship with tumour and treatment parameters. Radiother Oncol 41:55–59.

Hacker CD, Laumann TO, Szrama NP, Baldassarre A, Snyder AZ, Leuthardt EC, Corbetta M. 2013. Resting state network estimation in individual subjects. Neuroimage 82:616–633.

Harris RJ, Bookheimer SY, Cloughesy TF, Kim HJ, Pope WB, Lai A, et al. 2014. Altered functional connectivity of the default mode network in diffuse gliomas measured with pseudo-resting state fMRI. J Neurooncol 116:373–379.

Henke K, Weber B, Kneifel S, Wieser HG, Buck A. 1999. Human hippocampus associates information in memory. Proc Natl Acad Sci 96:5884–5889.

Hocke K, Kämpfer N. 2009. Gap filling and noise reduction of unevenly sampled data by means of the Lomb-Scargle periodogram. Atmos Chem Phys 9:4197–4206.

Ide JS, Li C-sR. 2011. A cerebellar thalamic cortical circuit for error-related cognitive control. Neuroimage 54:455–464.

Jensen CA, Chan MD, McCoy TP, Bourland JD, deGuzman AF, Ellis TL, et al. 2011. Cavity-directed radiosurgery as adjuvant therapy after resection of a brain metastasis. J Neurosurg 114:1585–1591.

Kovács Á, Emri M, Opposits G, Pisák T, Vandulek C, Glavák C, et al. 2015. Changes in functional MRI signals after 3D based radiotherapy of glioblastoma multiforme. J Neurooncol 125: 157–166.

Laukkanen E, Klonoff H, Allan B, Graeb D, Murray N. 1988. The role of prophylactic brain irradiation in limited stage small cell lung cancer: clinical, neuropsychologic, and ct sequelae. Int J Radiat Oncol Biol Phys 14:1109–1117.

Laumann TO, Gordon EM, Adeyemo B, Snyder AZ, Joo SJ, Chen MY, et al. 2015. Functional system and areal organization of a highly sampled individual human brain. Neuron 87:657–670.

Lawrence YR, Li XA, el Naqa I, Hahn CA, Marks LB, Merchant TE, Dicker AP. 2010. Radiation dose–volume effects in the brain. Int J Radiat Oncol Biol Phys 76(3, Supplement):S20–S27.

Logothetis NK, Pauls J, Augath M, Trinath T, Oeltermann A. 2001. Neurophysiological investigation of the basis of the fMRI signal. Nature 412:150–157.

Ma Q, Wu D, Zeng LL, Shen H, Hu D, Qiu S. 2016. Radiation-induced functional connectivity alterations in nasopharyngeal carcinoma patients with radiotherapy. Medicine 95:e4275.

Makale MT, McDonald CR, Hattangadi-Gluth JA, Kesari S. 2016. Mechanisms of radiotherapy-associated cognitive disability in patients with brain tumours. Nat Rev Neurol 13:52.

Marek S, Dosenbach NUF. 2019. Control networks of the frontal lobes. Handb Clin Neurol 163:333–347. DOI: 10.1016/B978-0-12-804281-6.00018-5

McDuff SGR, Taich ZJ, Lawson JD, Sanghvi P, Wong ET, Barker FG, et al. 2013. Neurocognitive assessment following whole brain radiation therapy and radiosurgery for patients with cerebral metastases. J Neurol, Neurosurg Psychiatry 84:1384.

Miezin FM, Maccotta L, Ollinger JM, Petersen SE, Buckner RL. 2000. Characterizing the hemodynamic response: effects of presentation rate, sampling procedure, and the possibility of ordering brain activity based on relative timing. Neuroimage 11:735–759.

Nasreddine ZS, Phillips NA, Bédirian V, Charbonneau S, Whitehead V, Collin I, et al. 2005. The montreal cognitive assessment, MoCA: a brief screening tool for mild cognitive impairment. J Am Geriatr Soc 53:695–699.

Ojemann JG, Akbudak E, Snyder AZ, McKinstry RC, Raichle ME, Conturo TE. 1997. Anatomic localization and quantitative analysis of gradient refocused echo-planar fMRI susceptibility artifacts. Neuroimage 6:156–167.

Power JD, Barnes KA, Snyder AZ, Schlaggar BL, Petersen SE. 2012. Spurious but systematic correlations in functional connectivity MRI networks arise from subject motion. Neuroimage 59:2142–2154.

Power JD, Cohen AL, Nelson SM, Wig GS, Barnes KA, Church JA, et al. 2011. Functional network organization of the human brain. Neuron 72:665–678.

Power JD, Mitra A, Laumann TO, Snyder AZ, Schlaggar BL, Petersen SE. 2014. Methods to detect, characterize, and remove motion artifact in resting state fMRI. Neuroimage 84:320–341.

Rypma B, Berger JS, Prabhakaran V, Martin Bly B, Kimberg DY, Biswal BB, D'Esposito M. 2006. Neural correlates of cognitive efficiency. Neuroimage 33:969–979.

Satterthwaite TD, Wolf DH, Loughead J, Ruparel K, Elliott MA, Hakonarson H, et al. 2012. Impact of in-scanner head motion on multiple measures of functional connectivity: relevance for studies of neurodevelopment in youth. Neuroimage 60:623–632.

Seeley WW, Crawford RK, Zhou J, Miller BL, Greicius MD. 2009. Neurodegenerative diseases target large-scale human brain networks. Neuron 62:42–52.

Seeley WW, Menon V, Schatzberg AF, Keller J, Glover GH, Kenna H, et al. 2007. Dissociable intrinsic connectivity networks for salience processing and executive control. J Neurosci 27:2349–2356.

Seitzman BA, Gratton C, Marek S, Raut RV, Dosenbach NUF, Schlaggar BL, et al. 2020. A set of functionally-defined brain regions with improved representation of the subcortex and cerebellum. Neuroimage 116290. doi:https://doi.org/10.1016/j.neuroimage.2019.116290

Sheffield JM, Kandala S, Tamminga CA, Pearlson GD, Keshavan MS, Sweeney JA, et al. 2017. Transdiagnostic associations between functional brain network integrity and cognition. JAMA Psychiatry 74:605–613.

Sheffield JM, Repovs G, Harms MP, Carter CS, Gold JM, MacDonald Iii AW, et al. 2015. Fronto-parietal and cingulo-opercular network integrity and cognition in health and schizophrenia. Neuropsychologia 73:82–93.

Sheline YI, Barch DM, Price JL, Rundle MM, Vaishnavi SN, Snyder AZ, et al. 2009. The default mode network and self-referential processes in depression. Proc Natl Acad Sci U S A 106:1942–1947.

Siegel JS, Mitra A, Laumann TO, Seitzman BA, Raichle M, Corbetta M, et al. 2017. Cereb Cortex 27:4492–4502. DOI: 10.1093/cercor/bhw253

Siegel JS, Ramsey LE, Snyder AZ, Metcalf NV, Chacko RV, Weinberger K, et al. 2016. Disruptions of network connectivity predict impairment in multiple behavioral domains after stroke. Proc Natl Acad Sci U S A 113:E4367.

Siegel JS, Snyder AZ, Metcalf NV, Fucetola RP, Hacker CD, Shimony JS, et al. 2014. The circuitry of abulia: insights from functional connectivity MRI. NeuroImage Clinical 6:320–326.

Smith SM, Jenkinson M, Woolrich MW, Beckmann CF, Behrens TE, Johansen-Berg H, et al. 2004. Advances in functional and structural MR image analysis and implementation as FSL. Neuroimage 23 Suppl 1:S208–S219.

Song M, Zhou Y, Li J, Liu Y, Tian L, Yu C, Jiang T. 2008. Brain spontaneous functional connectivity and intelligence. Neuroimage 41:1168–1176.

Swets JA, Tanner Jr WP, Birdsall TG. 1961. Decision processes in perception. Psychol Rev 68:301–340.

Tannock IF., Ahles TA, Ganz PA, van Dam FS. 2004. Cognitive impairment associated with chemotherapy for cancer: report of a workshop. J Clin Oncol 22:2233–2239.

Tsai PF, Yang CC, Chuang CC, Huang TY, Wu YM, Pai PC, et al. 2015. Hippocampal dosimetry correlates with the change in neurocognitive function after hippocampal sparing during whole brain radiotherapy: a prospective study. Radiat Oncol 10:253.

Welzel G, Fleckenstein K, Schaefer J, Hermann B, Kraus-Tiefenbacher U, Mai SK, Wenz F. 2008. Memory function before and after whole brain radiotherapy in patients with and without brain metastases. Int J Radiat Oncol Biol Phys 72:1311–1318.

Yan CG, Cheung B, Kelly C, Colcombe S, Craddock RC, Di Martino A, et al. 2013. A comprehensive assessment of regional variation in the impact of head micromovements on functional connectomics. Neuroimage 76:183–201.

Address correspondence to:
Timothy J. Mitchell
Department of Radiation Oncology
Washington University in St. Louis–School of Medicine
4921 Parkview Place #1
St. Louis, MO 63110

E-mail: tjmitchell@wustl.edu